Results in Engineering 22 (2024) 102241

Contents lists available at ScienceDirect

Results in Engineering

journal homepage: www.sciencedirect.com/journal/results-in-engineering

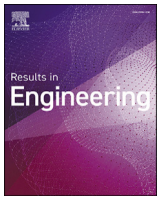

Research paper

Design and optimization of a siphon turbine using the response surface methodology

Juliana Guerra [a], Laura Velásquez [a,*], Ainhoa Rubio-Clemente [a,b], Leyla Jaramillo [c], Edwin Chica [a]

[a] Grupo de Energía Alternativa, Departamento de Ingeniería Mecánica, Facultad de Ingeniería, Universidad de Antioquia, Calle 70 No 52-21, Medellín 050010, Colombia
[b] Escuela Ambiental, Facultad de Ingeniería, Universidad de Antioquia, Calle 70 No 52-21, Medellín 050010, Colombia
[c] Grupo de Investigación en Tecnología y Medio Ambiente, Facultad de Ingeniería, Tecnológico de Antioquia Institución Universitaria, Calle 78b No 72A- 220, Medellín 050034, Colombia

ARTICLE INFO

Keywords:
Siphon turbine
Optimization
Response surface methodology
Renewable energy

ABSTRACT

A comprehensive examination of siphon turbine design and optimization using the response surface methodology (RSM) is presented in this study. The goal was to improve the turbine efficiency by analyzing the impact of two key factors: the number of blades (n) and the ratio between the hub diameter (d) and the outer diameter of the rotor (D), (d/D). The application of RSM facilitated the creation of a response surface, unveiling the optimal combination of factors for maximizing efficiency. The novelty of this article lies in utilizing the response surface methodology to refine the design of existing turbines, resulting in a more streamlined and effective design process tailored to the specific requirements of the installation. The findings indicated that rounding the number of blades to 5 and maintaining a constant d/D ratio of 0.35 yielded the highest efficiency (41.4%). Experimental validation was carried out and the accuracy of the optimized design was demonstrated, paving the way for practical applications in renewable energy solutions. Therefore, the effectiveness of RSM in optimizing siphon turbine designs is supported since valuable insights are provided for enhancing the energy efficiency in small-scale hydropower systems. The investigation contributes to the development of sustainable and clean energy technologies, showcasing the potential of siphon turbines in harnessing low-head water sources for power generation.

1. Introduction

Electric power has become an integral part of daily personal and business life, and its generation is one of the most challenging fields in engineering [1]. Technological advancements throughout history have heavily relied on a secure, reliable, and cost-effective electricity supply. In today's world, the demand for electric power is growing at an accelerated rate, necessitating sustainable generation methods. Non-renewable energy sources are those that exist in a limited quantity in nature, such as petroleum derivatives (coal, diesel, natural gas, fuel oil, etc.) and uranium [2,3]. Renewable energy sources (RES) have an inexhaustible potential as they originate from energy that continuously reaches the Earth due to solar radiation or the gravitational attraction of other planets and satellites in the solar system. The main RES include solar, wind, hydropower, tidal, geothermal, and biomass energy [4–6]. Currently, 70% of energy comes from non-renewable sources, while only 30% is renewable. The most employed non-renewable sources consisted of petroleum (33%), natural gas (25%), and coal (22%). As for the most prevalent renewable sources, they encompassed hydroelectric power (16%), wind energy (12%), and solar energy (10%) [7]. Among RES, hydroelectric power is the primary ally in generating clean energy due to its high predictability and availability [8]; its developments have a long lifespan of over 100 proven years, with possibilities for new designs and technological adaptations [9]. Within these new technological adaptations, siphon hydraulic turbines emerge. A siphon turbine is a low-head axial flow hydropower plant (HPP). In this type of turbine, water is transported from an upper tank to a lower tank using a siphon structure that passes over the dam structure. Its main advantage is the ability to adapt to existing structures where there is already a drop in water elevation, allowing the utilization of sites that were pre-

* Corresponding author.
E-mail address: lisabel.velasquez@udea.edu.co (L. Velásquez).

https://doi.org/10.1016/j.rineng.2024.102241
Received 31 January 2024; Received in revised form 22 April 2024; Accepted 7 May 2024
Available online 10 May 2024

Nomenclature

List of abbreviations

ANOVA	Analysis of variance
CFD	Computational fluid dynamics
Df	Degrees of freedom
GCI	Grid Convergence Index
HPP	Hydropower plant
PLA	Polylactic acid polymer
PVC	Polyvinyl Chloride
RES	Renewable energy sources
RSM	Response surface methodology
R^2	R-squared

List of symbols

η	Efficiency of the siphon turbine	
P_{out}	Generated power	W
P	Maximum available power	W
T	Total torque generated by the turbine	Nm
ω	Rotational speed of the runner	Rad/s
ρ	Density of the fluid	m^3/kg
g	Gravity	ms^2
Q	Volume flow rate	m^3/s
H	Difference in height between the fluid level in the upper and lower tank	m
V	Velocity of the water flow within the siphon	m/s
f	Friction factor	
L	Length of the pipe between the pools	m
D_p	is the diameter of the pipe	m
$\sum K$	Friction coefficients of the pipe fittings	
n	Number of rotor blades	
d	Hub diameter	m
D	Outer diameter of the rotor	m
N	Total number of runs or treatments	
k	Number of chosen factors	
b	Number of levels for each factor	
y	Dependent variable	

viously inaccessible with conventional hydraulic turbines. The siphon turbine has the potential to be used in decentralized energy systems, meaning in relatively smaller power generation facilities located closer to consumers, particularly in rural or remote areas. These turbines can harness local water sources and provide a clean and reliable source of electrical energy in locations where access to the power grid may be limited [10–12].

While the principle of siphon turbines was described over 35 years ago by Eller J.D. [13], the information available in the literature regarding this type of turbine is limited. Previous research has addressed various aspects of turbine design and operation, such as optimizing pipe geometry, selecting appropriate materials, and addressing challenges related to turbine startup and operational stability. Stark and coworkers explored the modeling and performance of a small siphonic hydropower system [14]. The research investigated the feasibility and efficiency of harnessing hydropower using a siphonic system in small-scale applications. The study focused on the development of a mathematical model to simulate the performance of the system and evaluate its power generation capabilities. The factors considered in their model were water flow rate, head height, and system efficiency. Experimental results were presented and compared with the model's predictions, demonstrating the reliability of their approach [14]. In turn, Loots et al. provided a comprehensive overview of various low-head hydropower technologies available, including turbine types, system configurations, and operational considerations [15]. The advantages and challenges associated with implementing low head hydropower systems were examined. The authors highlighted that the siphon turbine has as a potential solution for harnessing low-head hydropower in areas with limited water head [15]. In fact, Alidai et al. evaluated the feasibility and effectiveness of siphonic turbines in harnessing hydropower in low-head conditions and compared with traditional turbine designs [16]. A maximum efficiency of 7.2% was achieved for an available head of 1.25 m; therefore, the usability of siphon turbine depends on the head available [16]. Zhou and coworkers presented a study on the development of an ultra-low head siphon hydro turbine using computational fluid dynamics (CFD) [17]. The authors analyzed the flow characteristics and performance of the siphon hydro turbine under different operating condition considering factors such as head loss, flow velocity, and pressure distribution. The maximum hydraulic efficiency was found to be 87.9% under a head of 2.87 m (21.2 kW) [17]. Likewise, Martínez et al. conducted experimental investigations to analyze the performance characteristics and operational parameters of the siphon turbine under various flow conditions and head levels. For a head of 5.0 m, the turbine produced 159 kW of power [13]. Recently, Krylo et al. presented the methodology and setup used for the experimental studies, including the measurement of power output, efficiency, and operational parameters. The authors discussed the performance characteristics of the micro-hydropower plants with the siphon water intake system under various flow conditions and head levels and analyzed the influence of different parameters, such as flow rate, head height, and turbine configuration, on the performance and efficiency of the micro HPP. During experiments, five-bladed runners with an installed capacity of 30 kW were tested [18]. The number of blades in the rotors of siphon-type turbines can vary depending on the specific design and application requirements, i.e., there is not a fixed number that is universally common in all siphon turbines. Nevertheless, in general terms, siphon turbines typically have a relatively low number of blades compared to other types of turbines, due to their specific design and function.

Pizutti et al. conducted a study aiming to contribute alternatives for energy generation in existing low head dams through the predimensioning of a siphon plant. This plant type represents a specific and evolving niche for decentralized power generation. Among its favorable characteristics, reduced structural requirements and minimal intervention in dam structures are included. Therefore, socio-environmental, and economic impacts are mitigated. Different hybrid systems were simulated to determine an optimal configuration based on net present cost. The most promising solution involved a hybrid system comprising siphon turbines, photovoltaic modules, and a diesel support system, with an energy cost of 0.164 per kWh [19]. Krylov et al. conducted experiments on a scale model of a micro hydropower plant with a siphon water intake and a five-bladed Darrieus turbine, obtaining the characteristics of the power equipment within the available pressure and flow ranges. During the tests, the flow varied from 0.6 m^3/s to 1.4 m^3/s. The maximum efficiency achieved was 58.78% for a flow rate of 1.255 m^3/s, equivalent to a velocity of 2.6 m/s [18]. Volkov et al. proposed a scheme for the combined energy supply of an autonomous consumer based on a micro hydropower plant with a built-in axial turbine in the siphon-type penstock. This type of scheme allows for stable and reliable operation within the daily cycle, as well as the use of several hydraulic units of various power capacities as emergency backup. The authors developed a method for the preliminary evaluation of the efficiency of the hydraulic part of the energy complex. Losses in the penstock were taken into account, which allows predicting the energy characteristics of the complex at an early stage of design. Additionally, they conducted calculation, numerical, and experimental studies of the model and mockup

of the hydraulic unit to obtain its energy characteristics and verify its reliability [20].

The present investigation focuses on the hydrodynamic optimization of a small-scale siphon turbine using response surface methodology (RSM) and Computational fluid dynamics (CFD) simulation. The turbines studied in previous studies were turbines with a generation capacity exceeding 20 kW. Crucial geometric factors that impact the turbine design, such as the number of blades and the ratio between hub diameter and rotor diameter, are analyzed. Also, the influence of each chosen geometric factor on the turbine efficiency, which is the objective to be maximized, is being examined. Evaluating the influence of the factors and their simultaneous effects on turbine efficiency allows for the determination of the optimal treatment, i.e., the configuration that achieves the highest efficiency.

The innovative approach presented in this article lies in the utilization of advanced statistical models, particularly response surface models, to optimize the geometry of a siphon turbine. By employing sophisticated statistical techniques, it becomes possible to unravel the intricacies of the turbine's design parameters, systematically exploring a predefined design space. This optimization methodology not only facilitates the identification of optimal geometric configurations but also ensures the turbine's compatibility with the unique operational characteristics of a siphon-driven energy generation system. The integration of statistical modeling into the turbine design process represents a paradigm shift, providing a robust and efficient means to achieve superior performance in hydropower installations, ultimately contributing to the advancement of sustainable energy solutions.

2. Methods and materials

2.1. Siphon turbine fundamentals

Siphon turbines are a type of axial flow HPP that can be adapted to existing structures where there is already a drop in water elevation [5], as shown in Fig. 1. This type of turbine uses a partially submerged pipe to create a vacuum that draws water upwards and through it. The kinetic energy of the moving water drives the blades of the turbine, generating torque. This torque is transmitted through the turbine shaft to the generator, where it is converted into electrical energy. Siphon turbines have blades like Kaplan turbines and can process a predetermined design flow rate. However, a portion of the hydraulic power is lost due to viscous forces and losses in seals, bearings, and mechanical transmission. Moreover, the turbine requires approximately 30 to 60 s to initiate its operation, within this time frame, the generator acts as an electric motor that pumps water into the siphon until it is primed, after which it starts operating as a generator [15].

The performance of the siphon turbine depends on several factors, such as the pipe and the blade geometries, the rotor placement, and the water flow. The performance equation of the siphon turbine is defined by Eq. (1) [21].

$$\eta = \frac{P_{out}}{P} = \frac{T\omega}{\rho g Q(H)} \tag{1}$$

where η is the efficiency of the siphon turbine, P_{out} refers to the generated power, P is the maximum available power, T is the total torque generated by the turbine, ω is the rotational speed of the runner, ρ is the density of the fluid, g stands for the gravity, Q is the volume flow rate, and H is the difference in height between the fluid level in the upper and lower tank.

2.2. Siphon turbine design

There are several designs of HPP with siphon turbines. The most relevant among them in practice differ from each other by the location of the turbine within the siphon, as shown in Fig. 2. From the state of the art, it was identified that configuration 1 is the most used among

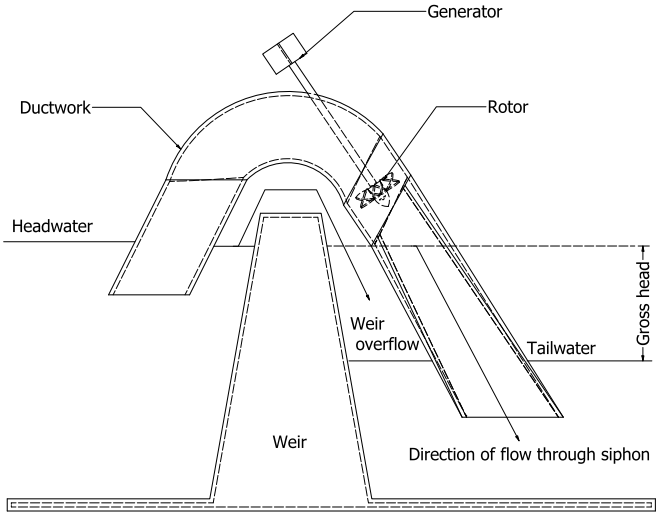

Fig. 1. Schematic diagram of a siphon turbine installed on a dam. Adapted from: [14].

the 6 configurations. This configuration served as the starting point for the hydraulic and structural design of the siphon turbine. To start the design, it is necessary to make some assumptions regarding the selected siphon configuration, as depicted in Fig. 3. These assumptions include:

- The hydraulic energy source consists of two pools or tanks, the upper and the lower one.
- The volumes of both tanks are infinitely large, assuming that water levels in both tanks remain unchanged during siphon operation.
- The pressure at the tank surfaces is equal to atmospheric pressure.

To determine the velocity (V) of the water flow within the siphon, Eq. (2) is employed [23,24].

$$V^2 = \frac{2gH}{f\left(\frac{L}{D_p}\right) + \sum K} \tag{2}$$

where f is the friction factor, L is the length of the pipe between the pools, D_p is the diameter of the pipe, and $\sum K$ represents the friction coefficients of the pipe fittings. Eq. (2) is derived from the Bernoulli equation [25] applied between the upper and the lower pools with the established assumptions.

Based on the specific attributes of an alternative energy pumping station at Universidad de Antioquia, a value of 0.85 m is established for H and a flow rate of 0.010 m^3/s ($P = 83.3$ W). In accordance with the basic parameters of the station, the diameter, shape, and material of the pipe were also selected. The siphon pipe is divided into several sections: an ascending section, a curve, a straight section, a new curve, and a descending section. The pipe parameters are as follows: the diameter is 4 inches SCH 40, the length of the ascending duct is 0.247 m, the angle of the curve sections is 90°, and the lengths of the straight and descending ducts are 0.19 m and 0.845 m, respectively. Polyvinyl Chloride (PVC) was chosen as the manufacturing material. For the rotor design Fig. 4, a Kaplan turbine was used as a basis. The rotor diameter is 0.085 m while its height is 0.02 m. The outer diameter was adjusted to match the siphon pipe diameter of 4 inches (0.1 m). The rotor has 6 blades of constant thickness (2.5 mm) evenly distributed around the central hub. The blades have an inlet angle and outlet angle of 64° and 35°, respectively. The angles of the base geometry were taken from Chan and Aung [26].

Historically, optimization endeavors have typically leaned on the one-factor-at-a-time (OFAT) method, wherein individual design parameters are altered independently to assess their isolated impacts on the performance of the process or the device to be optimized. Nonethe-

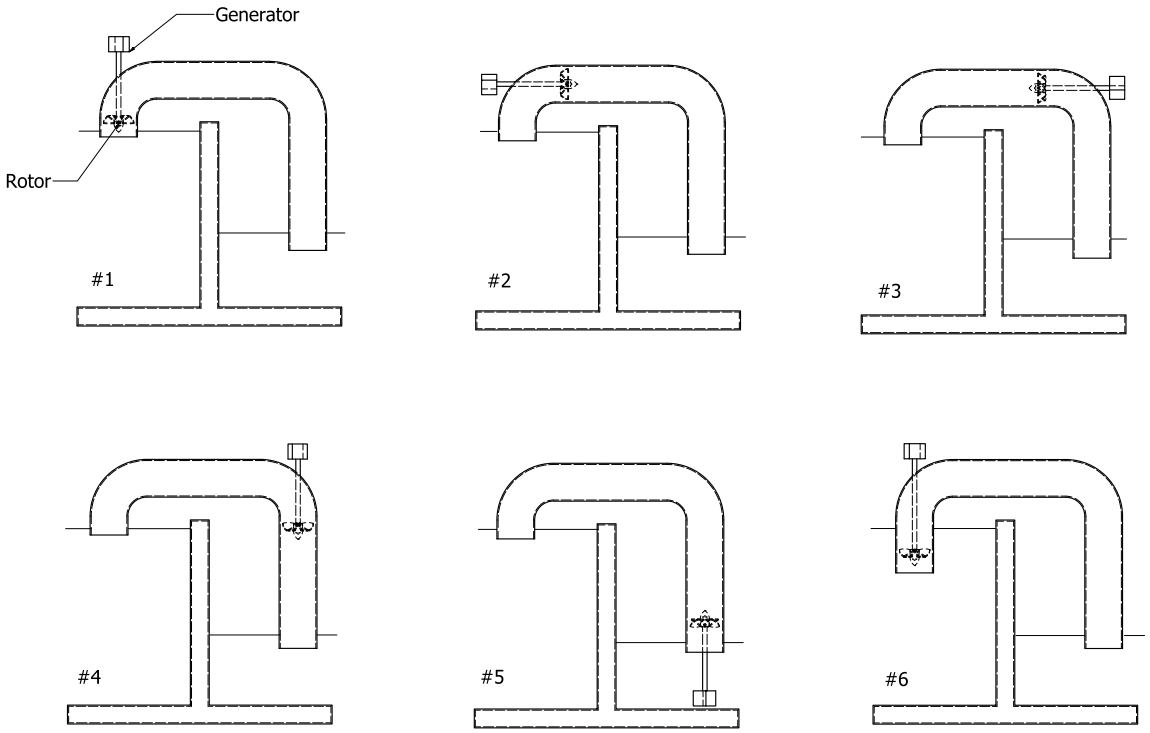

Fig. 2. Different designs of hydropower plants with siphon turbines. Adapted from: [22].

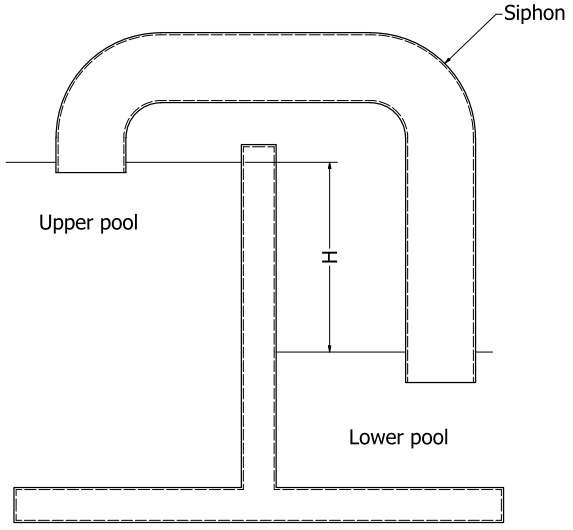

Fig. 3. Selected siphon configuration parameters. Adapted from: [22].

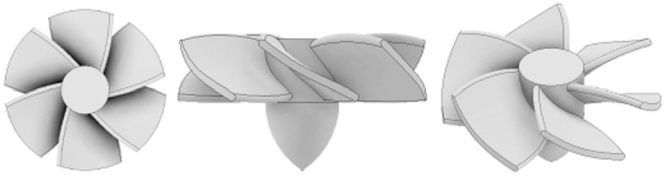

Fig. 4. Rotor of the siphon turbine design.

less, this approach often disregards potential interactions and synergies among multiple factors influencing the process or the device efficiency. This study promotes the adoption of the response surface methodology (RSM) as an alternative technique for the siphon turbine optimization. RSM takes a holistic approach, concurrently evaluating the interplay of various factors. By embracing RSM, intricate relationships can be revealed, and the optimal configurations can be identified, which might remain aside when conducting OFAT techniques [27,28].

The meticulous selection of independent variables, representing the design parameters impacting the device performance, is a crucial aspect of the RSM efficacy. These variables span diverse factors such as the blade geometry, rotational speed, fluid properties, and the structural considerations. Equally vital when RSM is carried out for optimization purposes is defining the response variable to be optimized, which could entail the power output, efficiency, or other pertinent performance metrics. The interdependency of these factors and their influence on the chosen response variable requires a comprehensive optimization strategy [29–31,28,32].

The following section provides further details of the RSM used for the design optimization of the siphon turbine.

2.2.1. Response surface methodology

RSM is a mathematical and statistical tool used in engineering to model and optimize relationships between input variables and response variables [33,34]. It is based on constructing a mathematical model that describes the relationship between the input variables and the desired response through a response surface function. This methodology allows for the exploration and analysis of the simultaneous effects of multiple variables, identification of optimal conditions for maximizing or minimizing the desired response, and optimization of process or system performance. The response surface is visualized as a three-dimensional surface that represents the relationship between the input variables and the response. Through this graphical representation, it is possible to identify trends, patterns, and optimal within the design space. Additionally, the response surface methodology enables sensitivity analysis to determine the relative influence of each variable on the response and makes predictions about the system's behavior in unexplored regions [35]. This methodology is applied in various engineering areas, such as industrial process optimization, product design, experimental design planning, quality improvement, materials engineering, and computer simulation. The technique of experimental design is a systematic approach to plan and conduct experiments with the objective of analyzing the effect of different variables (or factors) on a response. One

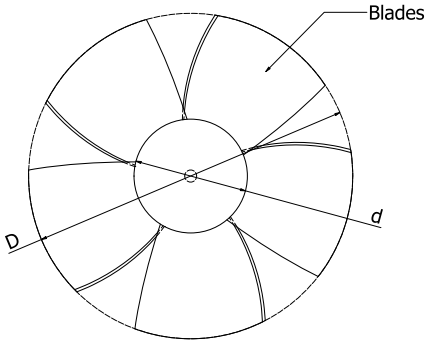

Fig. 5. Factors involved in rotor design.

Table 1
Independent factors and intervals employed in the optimization of the siphon turbine.

Independent factor	Values			Coded factor
	-1	0	+1	
Number of blades, n	4	5	6	x_1
Diameteŕs ratio, d/D	0.3	0.35	0.4	x_2

of the most used techniques in experimental designs is the full-factorial technique [35]. The full-factorial design is a strategy that allows exploring all possible combinations of levels of the variables of interest in an experiment. In this approach, all combinations of levels of each factor are tested, providing complete information on how individual factors and their interactions affect the response. The full-factorial design is particularly useful when it is expected that factors interact with each other, meaning that the effect of one factor may depend on the levels of other factors [36]. By including all possible combinations, it is possible to comprehensively evaluate and quantify both the main effects of the factors and their interactions. Moreover, by exploring all combinations, it is possible to identify optimal combinations of factor levels that maximize or minimize the desired response.

For the experimental design of this study, the number of rotor blades (n) and the ratio between the hub diameter (d) and the outer diameter of the rotor (D), d/D, were selected as the variables of interest, as shown in Fig. 5. Each chosen variable was explored at three different levels (-1, 0, and +1, representing low, medium, and high levels, respectively), as summarized in Table 1. For this investigation, the value of D was set at a constant 80 mm. It is essential to acknowledge the significance of the design parameters on the turbine performance such as the blade shapes, sizes, spacing, and the turbine housing, among others. Nevertheless, these factors were not considered during the optimization process. Only two factors were selected for the turbine optimization in order to reduce the number of experimental treatments. The analysis presented has specifically targeted parameters n and d/D due to their direct impact on the primary objective of the study. The remaining geometric factors that define the geometry of the turbine were determined based on the literature review.

In a complete factorial design, the total number of runs or treatments (N) related to the response variable can be calculated as illustrate in Eq. (3), where k represents the number of chosen factors and b refers to the number of levels for each factor [35]. Consequently, for the optimization of the current study, involving 2 factors with 3 levels each, the total number of treatments was 9. Table 2 displays the values of the independent factors for each of these treatments, while Table 3 shows the 3D view of each model.

$$N = b^k \tag{3}$$

At the end of the 9 tests, which were randomly run, a mathematical model (regression model) was established using the data derived from the simulation. In the regression model, the dependent variable represents the focus of investigation or prediction, while the independent variables are the ones used to explain or predict the dependent variable. The objective of the regression model is to determine the functional relationship between these variables. It is worth mentioning that various functions are available for constructing regression models, including linear, quadratic, cubic, and other specialized functions. However, in engineering applications where function approximation is common, second-order polynomial regression models are often preferred. These models effectively capture the main effects of independent variables and their interactions on the response variable. Additionally, within the turbine design, second-order response surfaces are extensively employed [37,38,27,39,40]. Hence, the decision to construct second-order regression models in this study was based on these considerations. Furthermore, an examination of the numerical results indicated a quadratic curvature in the efficiency values achieved, further justifying the use of second-order models. Eq. (4) describes the general expression representing a polynomial regression model [41,35,33].

$$y = \beta_0 + \beta_1 x_1 + \beta_2 x_2 + \beta_{11} x_1^2 + \beta_{22} x_2^2 + \beta_{12} x_1 x_2 \tag{4}$$

where, y refers to η, which was maximized; β_0 is a constant term; β_1 and β_2 are associated with the linear factors being examined; β_{11} and β_{22} stand for the quadratic coefficients, and β_{12} is the coefficient representing the interaction effects. A variance study, also known as analysis of variance (ANOVA), is a statistical technique used to analyze variability in data and determine if there are significant differences between the means of two or more groups or treatments [34]. This type of study is useful when comparing and evaluating the influence of different variables or factors on a variable of interest. ANOVA will allow to complement the information obtained from the regression model.

In statistical analysis, it is crucial to grasp and utilize terms such as the correlation coefficient (R^2) and the determination coefficient adjusted by the degrees of freedom (Adjusted-R^2). These metrics are essential for evaluating the accuracy and efficacy of the statistical models constructed, particularly in scenarios involving multiple variables and intricate relationships. R^2 provides insights into the level of correlation between the independent factors and the response variable considered, indicating how well the model accounts for the observed variations in the data obtained. Conversely, Adjusted-R^2 plays a critical role in preventing overfitting, ensuring that the model performance extends beyond the specific dataset it was trained on. By carefully understanding and interpreting these statistical indicators, researchers and analysts can make informed decisions regarding model selection, variable inclusion, and the overall reliability of the results. [40,28,32].

Upon determining the most appropriate model to express the behavior of the response variable and formulating the mathematical expression linking the explanatory and the response variables, the regression analysis progresses to validate critical hypotheses. Several assumptions must be met in regression analysis to ensure the accurate application of the regression model explaining the studied phenomenon [40,28,32].

Firstly, a correct model specification is essential, ensuring that the selected model accurately reflects the underlying relationship between the independent and dependent variables. Various statistical tools, including goodness-of-fit tests and residual analysis, are employed to evaluate the appropriateness of the model specification.

Additionally, the normality of residuals assumption dictates that the differences between the observed and the predicted values should follow a normal distribution. Deviations from this distribution can impact the validity of statistical tests and confidence intervals, requiring verification through statistical tests or visual inspections. When data deviate from a normal distribution, data transformation might be conducted. Transformations involve methods intended to modify the distribution of data to better align with a normal distribution or to stabilize variance. Common transformations include logarithmic, square root, and inverse of the response variable, among other transformations. The se-

Table 2
DOE design matrix. Experimental and predicted responses for the transformed (reduced) regression model.

Run	Number of blades, n (x_1)	Diameterś ratio, d/D (x_2)	Regression model	
			Efficiency of the CFD results (%)	Efficiency of the predicted results (%)
1	6	0.30	38.10	38.46
2	4	0.35	33.17	33.79
3	6	0.40	39.39	38.61
4	5	0.30	35.59	38.98
5	6	0.35	38.88	39.28
6	5	0.40	38.17	39.13
7	4	0.40	33.49	33.36
8	5	0.35	41.40	39.84
9	4	0.30	33.76	33.27

Table 3
Analyzed models.

Run 1	Run 2	Run 3
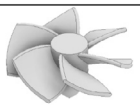	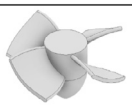	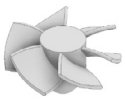
Run 4	**Run 5**	**Run 6**
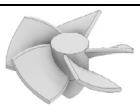		
Run 7	**Run 8**	**Run 9**
		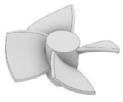

lection of the transformation is based on the data characteristics and the distancing degree from normality [40,28,32].

Furthermore, the absence of autocorrelation among residuals is crucial, indicating that residuals should not exhibit correlations with each other. Diagnostic plots and statistical tests are utilized to assess autocorrelation, as its presence can lead to inefficient parameter estimates and invalidate hypothesis tests [40,42,32].

Lastly, the assumption of constant variance of residuals (i.e., homoscedasticity) stipulates that the spread of residuals remains consistent across different predictor variable values. Verification of homoscedasticity is conducted through residual plots and statistical tests to ensure that variability does not systematically change with predictor variables [40,28,42].

Thorough validation of these assumptions is integral to regression analysis, ensuring the reliability of results and interpretations. Ignoring violations of these assumptions may result in biased parameter estimation, erroneous inferences, and unreliable predictions, emphasizing the significance of diligent validation in regression analysis.

2.3. Numerical simulation

To assess the influence of n and d/D on the performance of the siphon turbine, computational simulations were conducted using CFD. The ANSYS 2023 R2 Fluent software was employed for these simulations. The 3D computational domain comprised three distinct subdomains: two fixed subdomains representing the inlet and outlet flow conduits, and one moving subdomain containing the rotor. Fig. 6 illustrates the subdomains and boundary conditions.

As boundary conditions, a uniform velocity of 1.2 m/s and a turbulence intensity of 10% were imposed at the inlet. A relative pressure of 0 Pa was set at the outlet. The pipe walls were assigned a no-slip condition. Interface boundary conditions were employed between the

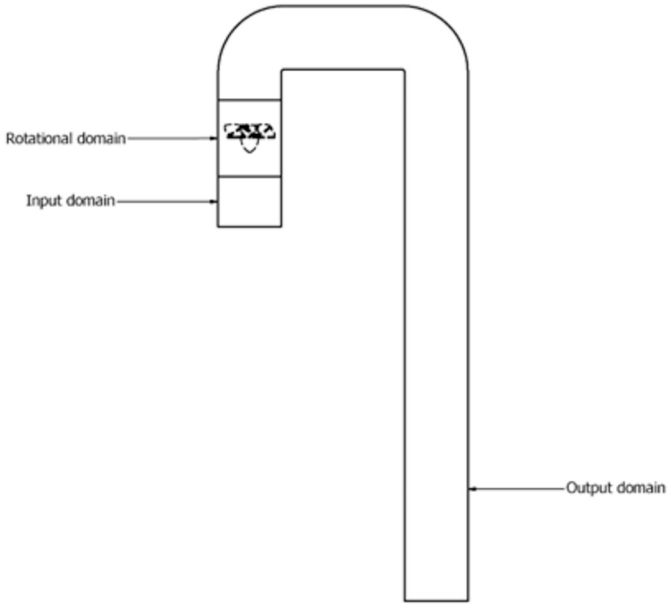

Fig. 6. Computational domains for ANSYs Fluent software simulation.

fixed and moving subdomains to ensure fluid continuity. The reference system originated from the center of the rotor. The simulation began with the rotor initially at rest, followed by the imposition of an angular velocity of 700 RPM. This change in velocity led to a corresponding change in the torque value. The $k-\omega$ SST turbulence model was utilized as the turbulence model. The selected turbulence model is widely favored for the rotor turbine modeling due to its proven superiority in handling complex flows, particularly those characterized by adverse pressure gradients and flow separations, typical in siphon turbines. Compared to standard k-ω and k-ϵ models, this turbulence model, as established by [43], exhibits enhanced predictive capabilities, especially in near-wall regions where adverse pressure gradients are prevalent. Numerous researchers have embraced the $k-\omega$ SST turbulence model for rotor turbine design purposes [41,40]. The mesh was generated using the Fluent meshing solver of ANSYS. The mesh refinement focused on the rotor surface to strike a balance between solution accuracy and computational costs. Fig. 7 represents an example of the mesh utilized in the numerical simulations.

A mesh independence study in numerical simulations is conducted to assess the sensitivity of the simulation results to the grid or mesh resolution. It involves varying the mesh size keeping other simulation parameters constant. The purpose of this study is to determine the minimum mesh resolution required to achieve accurate and reliable results. The Richardson extrapolation method and the Grid Convergence Index (GCI) are often employed in mesh independence studies. The Richardson extrapolation method is a numerical technique used to estimate the error reduction that can be achieved by refining the mesh, while the

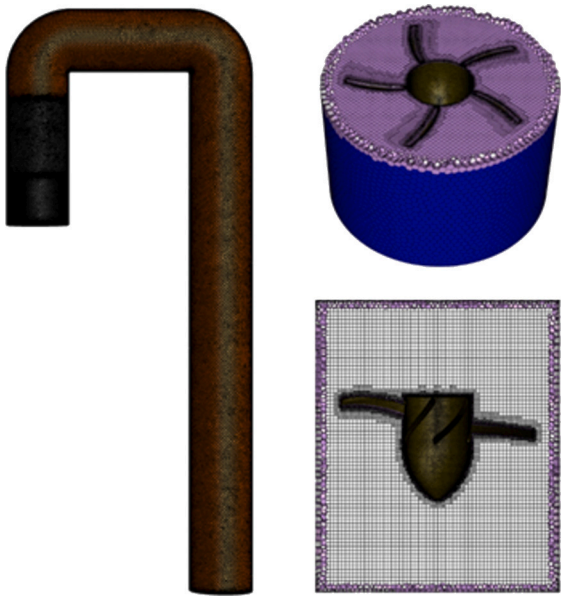

Fig. 7. Rotational and stationary domain meshes.

Table 4
Mesh characteristics.

	Coarse mesh	Medium mesh	Fine mesh
Number of nodes	1738035	3205821	7196334
Number of elements	635571	1115504	2586812
Max skewness	0.649	0.663	0.65
Max aspect ratio	23.61	28.97	23.35
Min orthogonal quality	0.351	0.337	0.35

Table 5
Grid convergence index (GCI).

	Mesh type	Number of elements	η (%)	Δ t (s)	η (%)
1	Coarse	635571	36.86	0.002	40.63
2	Medium	1115504	41.40	0.001	41.03
3	Fine	2586812	41.74	0.0005	41.40
	GCI_{12}	0.00082		0.13778	
	GCI_{23}	0.01109		0.15029	

Grid Convergence Index (GCI) quantifies the improvement in numerical accuracy as the mesh refinement is performed [44,45]. A smaller GCI value indicates a greater convergence and, therefore, a higher reliability in the numerical results [25]. This information helps in selecting an appropriate mesh size that provides accurate results while minimizing computational resources. The mesh characteristics utilized for the independence study are presented in Table 4.

Fig. 8 illustrates the results obtained from the independence tests and the solutions derived through the Richardson extrapolation. The values utilized for calculating the GCI are presented in Table 5.

A GCI close to zero in the Richardson extrapolation method serves as an indicator that the numerical results are highly accurate, signifying successful convergence in the simulation. In this analysis, two $GCIs$ were computed: GCI_{12} was employed to compare results between the finest mesh (Mesh 1) and the medium mesh (Mesh 2), while GCI_{23} compared results between the medium mesh (Mesh 2) and the coarsest mesh (Mesh 3). Both GCIs were also calculated for the time step (Δt). Based on the values presented in Table 5 for GCI_{12} and GCI_{23}, for both mesh and Δt, it is suggested that the results are reliable and closely approximate the exact solution to the problem. All simulations were carried out using a LENOVO Thinkstation P520 equipped with an Intel Xeon W2145 processor running at 3.7 GHz, coupled with 64 GB of RAM, operating in parallel, and employing 16 CPU cores.

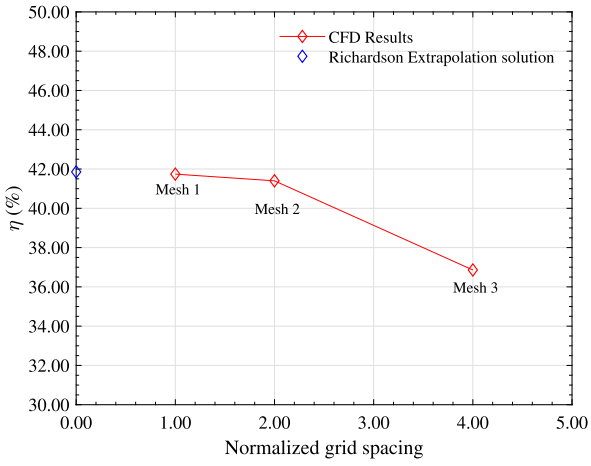

(a) Mesh independency test

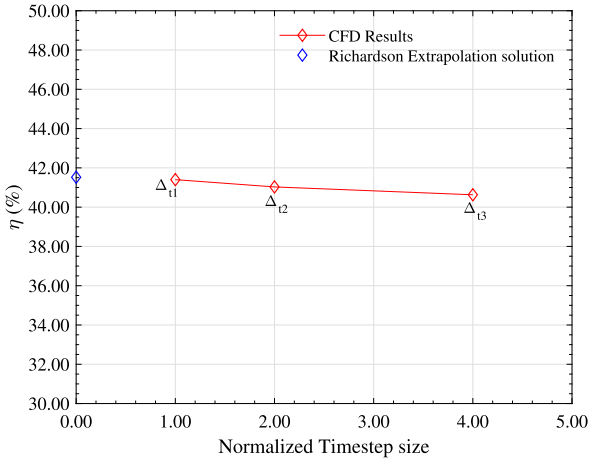

(b) Time-step independence test

Fig. 8. Independence tests.

3. Results and discussion

The CFD results obtained from the 9 treatments are shown in Table 2. From Table 2, the maximum efficiency value was achieved through treatment 8 ($d/D = 0.35$ and $n = 5$), reaching an efficiency of 41.4%. Fig. 9 shows the velocity and pressure distributions for treatment 8.

The analysis of pressure and velocity distribution provides crucial insights into the turbine's performance. This pressure-velocity relationship is indicative of efficient energy conversion within the turbine, demonstrating its ability to harness the kinetic energy of the fluid and convert it into useful mechanical or electrical energy, which is a pivotal outcome in the design and optimization of siphon turbines. From Fig. 9, it is evident that there is a high-pressure value before the flow passage through the rotor, followed by a corresponding pressure decrease after the rotor. In a siphon turbine, the fact that water pressure is high before entering the rotor and decreases after passing through it indicates that the rotor is effectively performing its role of converting the water energy into rotational mechanical energy. As water flows towards the rotor with high pressure, the rotor acts as a device that extracts a portion of this energy in the form of rotational motion, leading to a reduction in water pressure. This rotational mechanical energy can be harnessed to drive a generator for electricity generation.

In a siphon turbine, the transition from high water pressure upstream of the rotor to a lower pressure downstream indicates the ef-

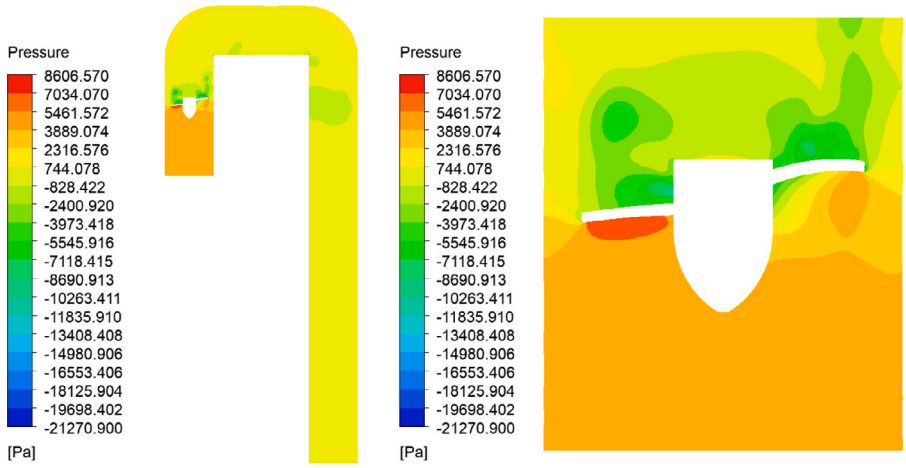

(a) Pressure distribution.

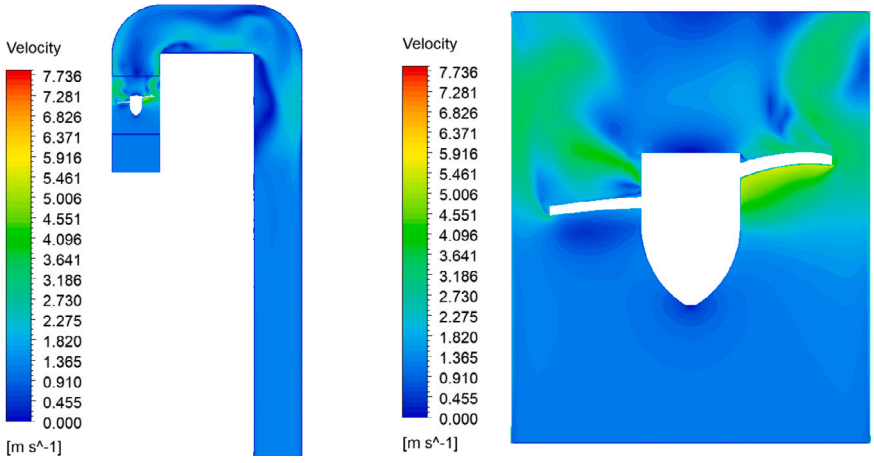

(b) Velocity distribution.

Fig. 9. CFD results.

fective conversion of water's energy into rotational mechanical energy by the rotor. As water flows toward the rotor under high pressure, the rotor functions as an apparatus to extract a portion of this energy, converting it into rotational motion. Consequently, this conversion process reduces the water pressure downstream of the rotor.

The ANOVA results obtained from the 9 treatments are shown in Table 6. Here, the values of sum of squares (Sum Sq), degrees of freedom (Df), mean square (Mean Sq), F-value, and p-value for each term in the model are compiled. The F-value indicates the ratio of explained variance to unexplained variance by the term. A large F-value indicates that the term has a significant influence on the data [34]. The p-value is the probability associated with the F-value and is used to assess statistical significance. A p-value lower than the chosen significance level (usually 0.05) indicates that the term is statistically significant [35]. The high F-value (17.89) and low p-value (0.008108) of the model indicate that the model is significant and explains a substantial amount of variability in the data. The terms x_1 and x_1x_1 have low p-values, indicating that these variables are individually significant in the model. On the other hand, the term x_2 has high p-values; therefore, it is not significant in the model. The "Residuals" variable represents the unexplained variation in the data and provides a measurement of the model fit quality. In the domain of experimental design utilizing RSM and ANOVA, the "residuals" variable has a pivotal importance as it serves as a crucial metric for gauging the unexplained variation inherent in the dataset. This unexplained variation can arise from diverse sources, such as measurement error, unaccounted-for variables, model misspecification, or inherent randomness within the system being investigated. While the main objective when fitting a model to the data is to capture as much variability in the response variable as possible using the predictor variables, it is imperative to acknowledge that any model can perfectly encapsulate all the intricacies of a real-world system. In the specific context of the response surface analysis, residuals represent the disparities between the observed data points and the values predicted by the fitted model. These discrepancies consider the portion of variation in the response variable that remains unexplained by the predictor variables incorporated into the model. Therefore, residuals serve as a valuable diagnostic tool, shedding light on the degree to which the model adequately accounts for the variability present in the data [42]. In this case, the residuals have a sum of squares of 6.360E-9. The R^2 value (94.71%) indicates the percentage of total variation explained by the model. A high R^2 indicates a better fit of the model to the observed data. Nevertheless, it is important to note that a high R^2 alone does not guarantee the validity of the model. The results from Table 6 correspond to a transformed and reduced regression model. A transformed regression model refers to an approach in regression analysis where transformations are applied to the independent and/or dependent variables to improve the linear relationship between them. The transformation is done using a mathematical function that modifies the original variable values. In this analysis, the response variable was transformed using a quadratic function and a reciprocal function. A reduced regression model refers to a regression model that contains a subset of variables from the full model. In other words, it is a model obtained by removing one or more

Table 6
Analysis of variance (ANOVA) for the transformed reduced regression model.

Term	Sum Sq	Df	Mean Sq	F-value	p-value
Model	$1.137E^{-7}$	4	$2.8439E^{-8}$	17.89	0.008108
x_1	$7.774E^{-8}$	1	$7.774E^{-8}$	48.909	0.00220
x_2	$4.000E^{-11}$	1	$4.000E^{-11}$	0.025	0.88295
x_1x_1	$3.469E^{-8}$	1	$3.469E^{-8}$	21.824	0.00951
$x_2\ x_2$	$1.290E^{-9}$	1	$1.290E^{-9}$	0.813	0.41810
Residuals	$6.360E^{-9}$	4	$1.590E^{-9}$		
R^2			94.71%		
Adjusted-R^2			89.41%		

Table 7
Regression models comparison.

	Model	p-value	R^2	Adjusted-R^2
I	Untransformed completed	0.05802	93.08%	81.54%
II	Untransformed reduced	0.01722	92.22%	84.84%
III	Transformed completed	0.0319	95.42%	87.79%
IV	Transformed reduced	0.008108	94.71%	89.41%

variables from the original, more complete model (Eq. (4)). For model reduction, variables with higher p-values were eliminated as they indicated non-significance in the model. In this case, only the interaction term between factors (x_1x_2) was removed. Table 7 shows the p-values, R^2, and adjusted-R^2 for four analyzed models: I) Untransformed completed, II) Untransformed reduced, III) Transformed completed and IV) Transformed reduced. Model I is not a valid model as the p-value is greater than 0.05. Although Model II has a p-value lower than 0.05, the values of R^2 and adjusted-R^2 were low, so a transformation of the response variable was sought to increase these values. Model III increased the values of R^2 and adjusted-R^2, indicating a better fit to the data. A significant change in the p-value was observed between Models I and II when removing the x_1x_2 term. Therefore, for Model IV, in addition to the transformation, the interaction term was also eliminated, resulting in increased values of R^2 and adjusted-R^2, and a decreased p-value; therefore, model IV was the selected model for this analysis.

The estimated coefficients of the regression model IV are presented in Eq. (5).

$$\frac{1}{y^2} = 0.00575538 - 0.00143078x_1 - 0.00717017x_2 + 0.000131695x_1^2 + 0.0101701x_2^2 \quad (5)$$

To ensure the validity of the model, the residuals of the regression model need to be assessed to verify if the assumptions of independence, normality, and homoscedasticity are met. A normality test of the residuals in a regression model is a statistical tool used to verify whether the residuals of the model follow a normal distribution. Residuals represent the differences between observed values (CFD results) and the values predicted by the regression model. The normality of residuals helps ensure the accuracy and reliability of the estimates. If the residuals follow a normal distribution, it implies that the model errors have a symmetrical distribution around zero, and the data points are randomly scattered around the regression line [42]. The results of the normality tests are displayed in Table 8. If the p-value of the test is high ($p > 0.05$), it is assumed that the residuals follow a normal distribution, supporting the normality assumption of the regression model. If the p-value of the test is low ($p < 0.05$), it indicates that the residuals do not follow a normal distribution, suggesting that the regression model may not be suitable for the data. According to the results in Table 8, the residuals of the model meet the normality assumption based on the employed tests. The normality assumption can also be assessed graphically, as demonstrated in Fig. 10. A graphical test of the normality assumption in a regression model involves visually inspecting a plot of the residuals to determine if they roughly follow a normal distribution. This assessment is done

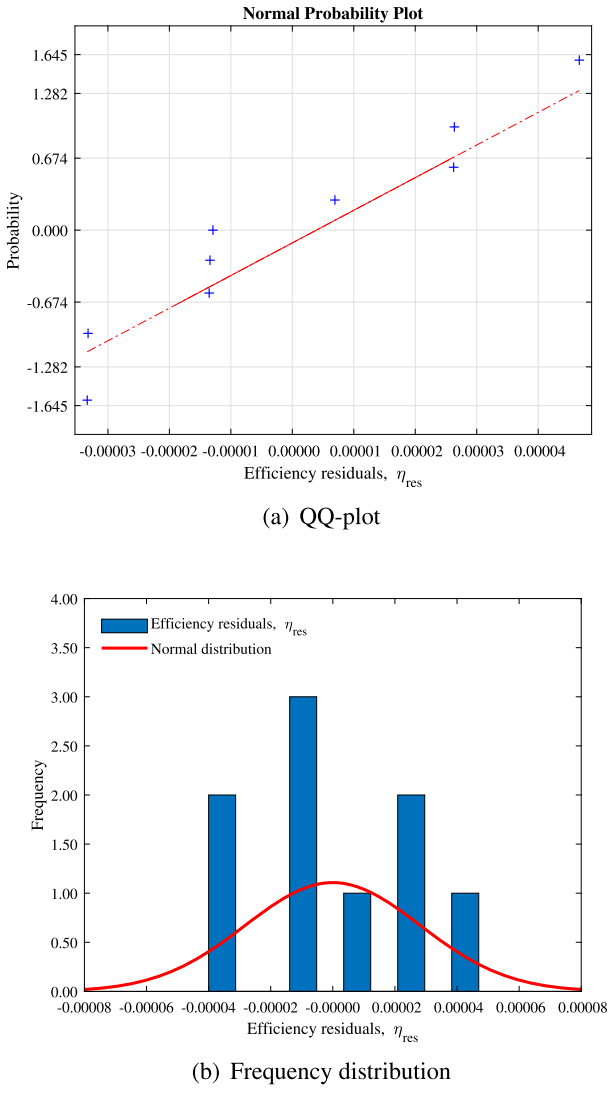

(a) QQ-plot

(b) Frequency distribution

Fig. 10. Graphical test of the normality.

through a quantile-quantile plot (QQ-plot) and/or a histogram of the residuals. The QQ-plot compares the quantiles of the residuals with the expected quantiles from a normal distribution [34]. When the residuals follow a normal distribution, the points on the plot will roughly align along a straight red line. The histogram displays the distribution of the residuals, and if they are normally distributed, the histogram should exhibit a bell-shaped symmetric pattern around zero. Graphical interpretation is subjective and relies on the analyst's experience. While QQ-plot analysis, as shown in Fig. 10(a), clearly demonstrates residuals aligning along the red straight line, the distribution in bell-shaped form is not as evident in the histogram, as seen in Fig. 10(b). Therefore, it is recommended to combine graphical analyses with formal statistical tests, as employed in Table 8, to obtain a more comprehensive assessment of the normality assumption in the regression model. The integration of statistical tests and graphical analyses provides a better understanding of the normality of the residuals and helps take appropriate decisions in regression analysis.

Once the normality assumption has been tested, it is necessary to check the assumptions of independence and homoscedasticity of the residuals. The assumption of independence of the residuals states that they should not exhibit systematic patterns or dependence in the order in which the data were collected. Independence of residuals implies that there is no relationship between errors in different observations. In other words, the error associated with a particular observation is

Table 8
Results of normality tests for the efficiency residuals.

Test	P-value
Shapiro-Wilk test	0.3728
Cramer-von Mises test	0.3034
KS Limiting form	0.6389
Shapiro-Francia test	0.4265
Jarque-Bera test	0.7114
Anderson-Darling test	0.3288
D'Agostino & Pearson test	0.6270
KS Lilliefors modification	0.1782

not affected by the errors of other observations. If this assumption is violated, it can lead to biased or imprecise results and may affect the validity of inferences made from the model [46,47]. To interpret the assumption of independence through statistical tests, methods like the Durbin-Watson test can be applied. A p-value lower than the significance level (0.05) suggests that the residuals may have autocorrelation, and the assumption of independence may not hold. With a p-value greater than the significance level, it is assumed that the residuals are independent. With a p-value of 0.8571, the independence assumption holds. The assumption of homoscedasticity, also known as equal variance, states that the dispersion of the residuals should be constant across all levels of the predictor variables. In other words, the variance of the residuals should not depend on the values of the independent variables. The Breusch-Pagan test, or BP test, is one of the most used statistical tests to assess the assumption of homoscedasticity in a regression model [42,46,47]. This test is applicable when there is suspicion that the variance of the residuals may not be constant across the range of values of the independent variables. The interpretation of the Breusch-Pagan test is also based on the p-value: If the p-value is greater than the significance level, it is assumed that the variance of the residuals is constant, and the assumption of homoscedasticity holds. If the p-value is less than the significance level, it is concluded that there is evidence of heteroscedasticity (non-constant variance) in the model. This suggests that the variance of the residuals is not constant, which can affect the precision of the estimates and the validity of the inferences from the model. With a p-value of 0.3014 for the BP test, the assumption of equal variances is met. After validating the regression model, it can be used to generate and plot a response surface. A response surface is a three-dimensional graphical representation used to visualize how a response variable (dependent) changes with two predictor variables (independent) in a regression model. The response surface for the obtained regression model is shown in Fig. 11.

From Fig. 11, it can be observed that the maximum value of the response variable (40.64%) occurs when n and d/D take the values of 5.4 and 0.35, respectively. However, from a physical standpoint, having a rotor with 5.4 blades is impossible. Therefore, to establish the optimal design for the siphon turbine, the number of blades was rounded to 5, while the d/D ratio remained constant at 0.35. For $n = 5$ and $d/D = 0.35$, the efficiency predicted by the model is 39.84%. This combination of values for the analysis factors corresponds to Treatment 8 of the initial simulations shown in Table 2. For a rotor with 6 blades, regardless of the d/D ratio, the efficiency does not change significantly, reaching an average value of 38.78%. For a rotor with 4 blades, the efficiency decreases significantly, but it is independent on d/D, with an average efficiency of 33.47%. According to the results of the ANOVA, Table 6, and the response surface, Fig. 11, analysis of the two analysis factors, n and d/D, the d/D ratio is not a significant factor. In other words, the efficiency is not affected by the changes in the d/D ratio. To validate the results of the regression model and computational simulations, experimental tests were conducted on the optimal model.

While RSM proved to be effective in identifying an optimal configuration by analyzing the influence of key factors such as n and the d/D ratio, the study primarily focused on these two factors, potentially

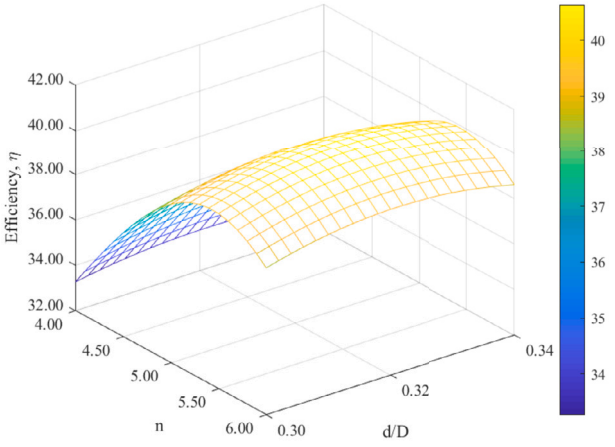

(a) Response surface plot for the efficiency: Effects of x_1 and x_2

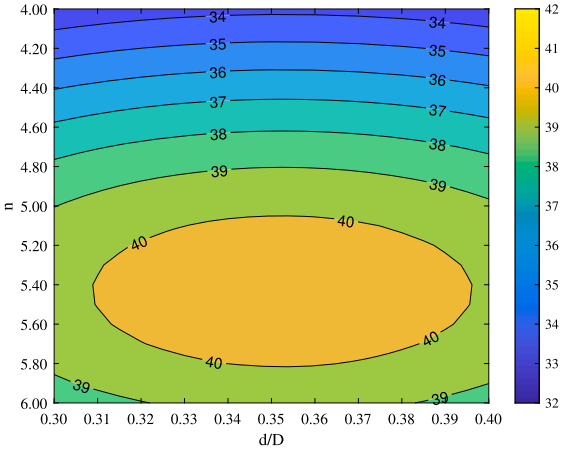

(b) Contour plot for the efficiency: Effects of x_1 and x_2

Fig. 11. Response surface and Contour plot for the efficiency.

overlooking other variables that could influence the turbine efficiency. Additionally, although RSM facilitated the determination of an efficient design, the findings may be limited in their generalizability to different turbine designs or operating conditions. While experimental validation supported the accuracy of the optimized design, the study scope may not encompass all possible real-world scenarios, requiring further validation under varied conditions to ensure robustness and applicability across a broader range of situations. Therefore, while the RSM approach showed promising results for optimizing siphon turbine designs, future research should consider exploring a wider variety of factors and conducting comprehensive validation to address potential limitations and enhance the reliability and applicability of the findings.

3.1. Experimental test

For the experimental tests, a 1:1 scale model of the optimized turbine was constructed using the additive manufacturing technique, also known as 3D printing. This technique enables the production of parts with complex geometries, providing a high-quality surface finish and excellent strength. The polylactic acid polymer (PLA) was chosen as the material for manufacturing the rotor, as it exhibits favorable mechanical properties and can operate in water without experiencing wear or degradation. Fig. 12 shows the rotor obtained through the 3D printing manufacturing process. Fig. 13 illustrates a section of the pumping station. The figure highlights an upward pipe section, an elbow, a straight

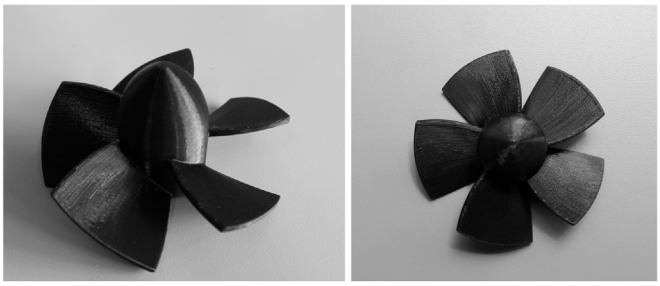

Fig. 12. 3D rotor.

segment, a second elbow, and a downward section. The experimental tests were executed under the condition of constant volume flow rate ($Q = 0.010\ m^3/s$). The angular velocity and total torque over the runner were measured with a rotary torque Sensor (Futek TRS 605-FSH02057). When the tests were started, the torque sensor reading is set to zero when the angular velocity is at its maximum. A variable load was imposed on the runner. The load was increased to reduce the angular velocity until 0 rpm. The load was controlled by an inverter and a motor. Knowing the flow rate, (Q) the difference height between the level of fluid in the upper and lower tank (H), the values of angular velocity (ω) and torque (T), the efficiency of the turbine is determined using Eq. (1).

Fig. 14 depicts the measured efficiency of the turbine across a range of angular velocities from 0 to 700 rpm for CFD data and up to 200 rpm for experimental data. While the experimental evaluation offers valuable insights into the rotor performance, it may be constrained, especially concerning higher angular velocities. Within the range between 0 and 200 rpm, both curves show significant similarities, affirming the credibility of the simulation results. The experimental siphon turbine did not attain high rotation speeds due to mechanical losses from friction between moving components like bearings, mechanical seals, and couplings, which were not factored into the computational simulations. Additionally, the experimental setup pump capacity limitations prevented reaching higher speeds, limiting a comprehensive understanding of the turbine behavior at those velocities. At high speeds, turbine vibrations may occur, potentially affecting the accuracy of the power measurements obtained using the torque sensor. These vibrations can introduce fluctuations in torque readings, leading to inconsistencies in the power measurement. As a result, the experimental performance curve of the turbine may deviate from the curve obtained through CFD simulations. The presence of vibrations can introduce additional mechanical forces and disturbances in the system, influencing the interaction between the turbine and the fluid flow.

The reliability of the experimental findings from the optimized turbine hinges on several critical factors, including the stability of operational conditions and the technical assumptions underlying the models of the study.

Firstly, the stability of the system operational conditions, namely the consistent maintenance of the water column height (H) and the flow rate (Q) during testing, is paramount. Variations in these parameters could lead to substantial fluctuations in the generated power and in the turbine rotation speed. By ensuring their stability, results that are not only consistent but also comparable can be obtained, facilitating a robust assessment of the turbine performance.

In addition, the technical assumptions embedded within the regression models play a pivotal role in the reliability of the findings. For instance, the dimensions and geometric specifications of the system components, including the pipe length and diameter, were meticulously selected according to predefined design requirements and operational parameters of the pumping system. These assumptions are fundamental as they form the basis for the regression models used to optimize the turbine design.

Moreover, the choice of materials for constructing the pipeline and the turbine rotor -PVC and polylactic acid (PLA) polymer, respectively- rests on the assumption that they possess the mechanical and environmental attributes necessary for an effective and safe operation within the intended application environment. These materials were selected based on their demonstrated ability to withstand hydraulic and mechanical stresses associated with the siphon turbine operation, as well as their resistance to degradation from exposure to water and other environmental factors.

Furthermore, the accuracy and precision of measurements, including the angular velocity and torque, conducted during experimental trials are essential for ensuring the reliability of the data obtained. It is assumed that these measurements were carried out meticulously using calibrated and dependable equipment, such as the Futek TRS 605-FSH02057 rotary torque sensor, thereby bolstering the credibility of the study conclusions.

In this regard, by carefully considering and addressing these critical factors and assumptions, the robustness and reliability of the experimental findings can be enhanced, providing a solid foundation for further analysis and interpretation within the field of the turbine design and optimization.

4. Conclusions

The RSM is a powerful and effective approach for designing and optimizing a siphon turbine. By utilizing the RSM, the impact of key factors, such as the number of blades (n) and the ratio between the hub diameter (d) and the outer diameter of the rotor (D), (d/D), on the turbine efficiency (η) was analyzed. The optimum design, with an efficiency of 41.4%, was achieved by rounding the number of blades to 5 and maintaining a d/D ratio of 0.35 from the optimization intervals of $4 < n < 6$ and $0.3 < d/D < 0.4$.

From the analysis of the response surface and ANOVA derived from the transformed and reduced regression model (Model IV), the d/D ratio was not a significant factor affecting the efficiency of the turbine under study. This finding indicates that the turbine performance can be optimized by adjusting the number of blades, which simplifies the design process.

Possible future research on this topic might involve assessing additional design parameters not previously considered. This may encompass aspects such as the blade shape or the aerodynamic profile. Additionally, investigating the turbine response to variable conditions, such as changes in the water flow velocity or variations in load; and integrating economic considerations into the optimization process, including the cost of materials used in the turbine construction, would allow for the development of a turbine design that is not only technically efficient but also economically viable.

CRediT authorship contribution statement

Juliana Guerra: Methodology, Investigation, Conceptualization. **Laura Velásquez:** Writing – original draft, Validation, Methodology, Investigation, Conceptualization. **Ainhoa Rubio-Clemente:** Writing – review & editing, Methodology. **Leyla Jaramillo:** Writing – review & editing. **Edwin Chica:** Writing – review & editing, Writing – original draft, Validation, Methodology, Investigation.

Declaration of competing interest

The authors declare that they have no known competing financial interests or personal relationships that could have appeared to influence the work reported in this paper.

Data availability

The authors are unable or have chosen not to specify which data has been used.

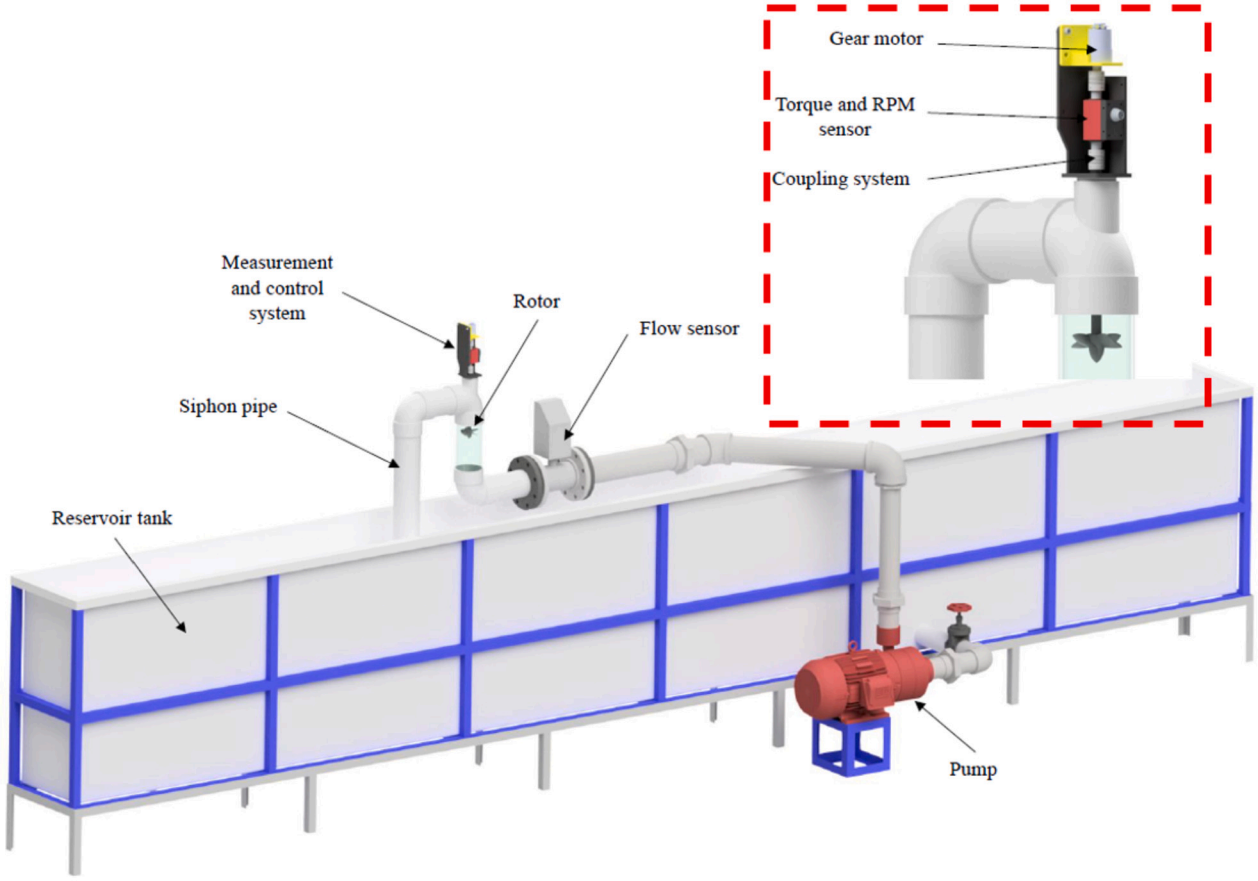

Fig. 13. Pumping Station.

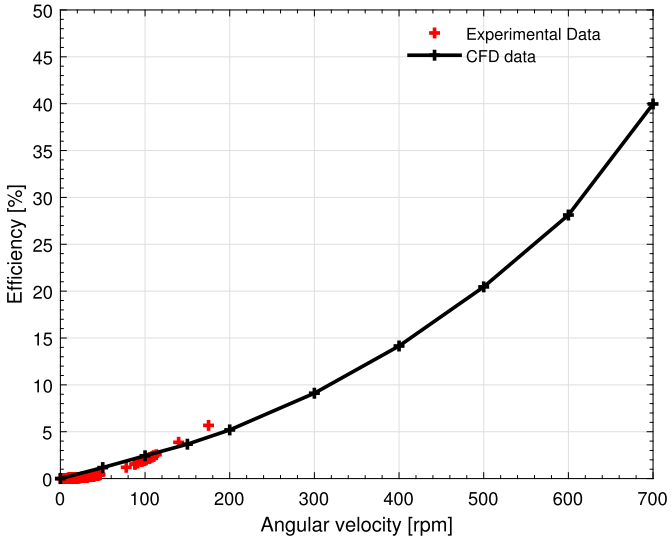

Fig. 14. Turbine performance curve. Efficiency vs. angular velocity.

Acknowledgements

Authors gratefully acknowledge the financial support provided by Universidad de Antioquia and Tecnológico de Antioquia, I.U. (Project No. 2022-52590).

References

[1] A.J. Wood, B.F. Wollenberg, G.B. Sheblé, Power Generation, Operation, and Control, John Wiley & Sons, 2013.

[2] D. Flórez-Orrego, J.A. Silva, S. de Oliveira Jr, Renewable and non-renewable exergy cost and specific co2 emission of electricity generation: the Brazilian case, Energy Convers. Manag. 85 (2014) 619–629.

[3] D.P. Kothari, R. Ranjan, K. Singal, Renewable Energy Sources and Emerging Technologies, 2021.

[4] E.T. Sayed, T. Wilberforce, K. Elsaid, M.K.H. Rabaia, M.A. Abdelkareem, K.-J. Chae, A. Olabi, A critical review on environmental impacts of renewable energy systems and mitigation strategies: wind, hydro, biomass and geothermal, Sci. Total Environ. 766 (2021) 144505.

[5] A. Rahman, O. Farrok, M.M. Haque, Environmental impact of renewable energy source based electrical power plants: solar, wind, hydroelectric, biomass, geothermal, tidal, ocean, and osmotic, Renew. Sustain. Energy Rev. 161 (2022) 112279.

[6] W.A. Eltayeb, J. Somlal, S. Kumar, S.K. Rao, Design and analysis of a solar-wind hybrid renewable energy tree, Results Eng. 17 (2023) 100958.

[7] P. Dechamps, The iea world energy outlook 2022–a brief analysis and implications, Eur. Energy Climate J. 11 (2023) 100–103.

[8] M.M. Kamal, A. Abbas, T. Alam, N.K. Gupta, R. Khargotra, et al., Hybrid cross-flow hydrokinetic turbine: computational analysis for performance characteristics with helical savonius blade angle of 135°, Results Eng. 20 (2023) 101610.

[9] C. Breyer, A global overview of future energy, Future Energy (2020) 727–756.

[10] C.S. Kaunda, C.Z. Kimambo, T.K. Nielsen, A technical discussion on microhydropower technology and its turbines, Renew. Sustain. Energy Rev. 35 (2014) 445–459.

[11] C.M. Niebuhr, M. Van Dijk, V.S. Neary, J.N. Bhagwan, A review of hydrokinetic turbines and enhancement techniques for canal installations: technology, applicability and potential, Renew. Sustain. Energy Rev. 113 (2019) 109240.

[12] R.K. Chaulagain, L. Poudel, S. Maharjan, A review on non-conventional hydropower turbines and their selection for ultra-low-head applications, Heliyon (2023).

[13] J.J. Martinez, Z.D. Deng, E.-M. Klopries, R.P. Mueller, P.S. Titzler, D. Zhou, B. Beirao, A.W. Hansten, Characterization of a siphon turbine to accelerate low-head hydropower deployment, J. Clean. Prod. 210 (2019) 35–42.

[14] B.H. Stark, E. Andò, G. Hartley, Modelling and performance of a small siphonic hydropower system, Renew. Energy 36 (2011) 2451–2464.

[15] I. Loots, M. Van Dijk, B. Barta, S. Van Vuuren, J. Bhagwan, A review of low head hydropower technologies and applications in a South African context, Renew. Sustain. Energy Rev. 50 (2015) 1254–1268.

[16] A. Alidai, I. Pothof, Hydraulic performance of siphonic turbine in low head sites, Renew. Energy 75 (2015) 505–511.

[17] D. Zhou, J. Gui, Z.D. Deng, H. Chen, Y. Yu, A. Yu, C. Yang, Development of an ultra-low head siphon hydro turbine using computational fluid dynamics, Energy 181 (2019) 43–50.
[18] A. Krylov, A. Bakshtanin, E. Beglyarova, Experimental studies of micro-hydropower plants with siphon water intake, Power Technol. Eng. 55 (2021) 321–325.
[19] J.T. Pizutti, C.H.P.A. Galdino, F.S.C. Meirelles, A. Beluco, Siphon-type hydroelectric plants: application for power generation in a low head dam in southern Brazil, J. Eng. Exact Sci. 10 (2024) 16392.
[20] A. Volkov, A. Ryzhenkov, A. Druzhinin, A. Vikhlyantsev, B. Orakhelashvili, V. Baikov, J. Šoukal, M. Sedlař, M. Komárek, F. Pochylỳ, et al., Application of New Approaches to the Hydropower Combined Complex Creation for Autonomous Energy Supply, E3S Web of Conferences, vol. 320, EDP Sciences, 2021, p. 04002.
[21] Y. Cengel, J. Cimbala, Ebook: Fluid Mechanics Fundamentals and Applications (si units), McGraw Hill, 2013.
[22] A.G. Parygin, A.V. Volkov, A.V. Ryzhenkov, Commentary on the efficiency of selected structural designs of low head micro hydraulic power plants, Mod. Appl. Sci. 9 (2015) 116.
[23] J. Zheng, J. Guo, J. Wang, Y. Zhang, Q. Lü, H. Sun, Calculation of the flow velocity of a siphon, Phys. Fluids 33 (2021).
[24] J. Zheng, J. Wang, J. Guo, Y. Zhang, Q. Lü, H. Sun, A siphon drainage system with variable diameters for landslides: concept, calculation, and validation, J. Hydrol. 597 (2021) 126305.
[25] R. Qin, C. Duan, The principle and applications of Bernoulli equation, J. Phys. Conf. Ser. 916 (2017) 012038, IOP Publishing.
[26] Z.M. Chan, Z.N. Aung, Design calculation of Kaplan turbine runner blade for 15kw micro hydropower plant, Int. J. Adv. Res. Dev. 5 (2020) 14–16.
[27] E. Gallego, A. Rubio-Clemente, J. Pineda, L. Velásquez, E. Chica, Experimental analysis on the performance of a pico-hydro turgo turbine, J. King Saud Univ., Eng. Sci. 33 (2021) 266–275.
[28] L. Velásquez, A. Posada, E. Chica, Optimization of the basin and inlet channel of a gravitational water vortex hydraulic turbine using the response surface methodology, Renew. Energy 187 (2022) 508–521.
[29] L.A. Gallo, E.L. Chica, E.G. Flórez, Numerical optimization of the blade profile of a savonius type rotor using the response surface methodology, Sustainability 14 (2022) 5596.
[30] J. Betancour, F. Romero-Menco, L. Velásquez, A. Rubio-Clemente, E. Chica, Design and optimization of a runner for a gravitational vortex turbine using the response surface methodology and experimental tests, Renew. Energy 210 (2023) 306–320.
[31] S.Z. Hosseini Imeni, A. Kaabinejadian, H. Ami Ahmadi, M. Moghimi, Optimal design and sensitivity analysis of airfoil-shaped rotor blade for savonius wind turbine by using response surface methodology, Wind Eng. 46 (2022) 1203–1223.
[32] L. Velásquez, A. Posada, E. Chica, Surrogate modeling method for multi-objective optimization of the inlet channel and the basin of a gravitational water vortex hydraulic turbine, Appl. Energy 330 (2023) 120357.
[33] R.H. Myers, D.C. Montgomery, C.M. Anderson-Cook, Response Surface Methodology: Process and Product Optimization Using Designed Experiments, John Wiley & Sons, 2016.
[34] E. George, W.G. Hunter, J.S. Hunter, Statistics for Experimenters: Design, Innovation, and Discovery, Wiley, 2005.
[35] C. Montgomery, Design and Analysis of Experiments, 8 edn, John Willey & Sons, Inc, New York, 2012.
[36] C.J. Wu, M.S. Hamada, Experiments: Planning, Analysis, and Optimization, John Wiley & Sons, 2011.
[37] H.S. Toft, L. Svenningsen, W. Moser, J.D. Sørensen, M.L. Thøgersen, Assessment of wind turbine structural integrity using response surface methodology, Eng. Struct. 106 (2016) 471–483.
[38] K. Gaiser, P. Erickson, P. Stroeve, J.-P. Delplanque, An experimental investigation of design parameters for pico-hydro turgo turbines using a response surface methodology, Renew. Energy 85 (2016) 406–418.
[39] P. Mojaver, S. Jafarmadar, S. Khalilarya, A. Chitsaz, Investigation and optimization of a co-generation plant integrated of gasifier, gas turbine and heat pipes using minimization of Gibbs free energy, Lagrange method and response surface methodology, Int. J. Hydrog. Energy 45 (2020) 19027–19044.
[40] F. Romero-Menco, J. Betancour, L. Velásquez, A. Rubio-Clemente, E. Chica, Horizontal-axis propeller hydrokinetic turbine optimization by using the response surface methodology: performance effect of rake and skew angles, Ain Shams Eng. J. 15 (2024) 102596.
[41] M. Bouvant, J. Betancour, L. Velásquez, A. Rubio-Clemente, E. Chica, Design optimization of an Archimedes screw turbine for hydrokinetic applications using the response surface methodology, Renew. Energy 172 (2021) 941–954.
[42] D.C. Montgomery, E.A. Peck, G.G. Vining, Introduction to Linear Regression Analysis, John Wiley & Sons, 2021.
[43] F.R. Menter, Two-equation eddy-viscosity turbulence models for engineering applications, AIAA J. 32 (1994) 1598–1605.
[44] H.K. Versteeg, W. Malalasekera, An Introduction to Computational Fluid Dynamics: the Finite Volume Method, Pearson Education, 2007.
[45] O.C. Zienkiewicz, R.L. Taylor, J.Z. Zhu, The Finite Element Method: Its Basis and Fundamentals, Elsevier, 2005.
[46] D.E. Hinkle, W. Wiersma, S.G. Jurs, et al., Applied Statistics for the Behavioral Sciences, vol. 663, Houghton Mifflin, Boston, 2003.
[47] A. Field, Discovering Statistics Using IBM SPSS Statistics, Sage, 2013.